Cell adaptive response to extracellular matrix density is controlled by ICAP-1–dependent β_1-integrin affinity

Angélique Millon-Frémillon,[1,2,3] Daniel Bouvard,[1,2,3] Alexei Grichine,[2,4] Sandra Manet-Dupé,[1,2,3] Marc R. Block,[1,2,3] and Corinne Albiges-Rizo[1,2,3]

[1]Institut National de la Santé et de la Recherche Médicale U823, [2]Université Joseph Fourier, [3]Centre National de la Recherche Scientifique, Equipe de Recherche Labellisée 3148, and [4]Cell Imaging Platform, Institut Albert Bonniot, 38042 Grenoble Cedex 9, France

Cell migration is an integrated process requiring the continuous coordinated assembly and disassembly of adhesion structures. How cells orchestrate adhesion turnover is only partially understood. We provide evidence for a novel mechanistic insight into focal adhesion (FA) dynamics by demonstrating that integrin cytoplasmic domain–associated protein 1 (ICAP-1) slows down FA assembly. Live cell imaging, which was performed in both *Icap-1*–deficient mouse embryonic fibroblasts and cells expressing active β_1 integrin, shows that the integrin high affinity state favored by talin is antagonistically controlled by ICAP-1. This affinity switch results in modulation in the speed of FA assembly and, consequently, of cell spreading and migration. Unexpectedly, the ICAP-1–dependent decrease in integrin affinity allows cell sensing of matrix surface density, suggesting that integrin conformational changes are important in mechanotransduction. Our results clarify the function of ICAP-1 in cell adhesion and highlight the central role it plays in the cell's integrated response to the extracellular microenvironment.

Introduction

Adhesion to ECM is primarily mediated by integrins, a family of heterodimeric receptors (Hynes, 2002) that cluster into adhesion sites. Focal adhesions (FAs) have been shown to form a scaffold that first sense and then transform extracellular cues into cellular responses and, in turn, transmit the contractile intracellular tensions to the ECM (Bershadsky et al., 2003; Ingber, 2003; Chen et al., 2004). Because of their involvement in cell motility and matrix remodeling, adhesion sites are necessarily dynamic structures that are able to assemble and disassemble. FA assembly takes place at the leading edge of membrane protrusions, whereas disassembly occurs both at the cell rear and at the base of protrusions. The molecular mechanisms controlling FA turnover have been partly characterized. They require Rho family GTPases, integrin engagement, and coordinated interaction between integrins and structural/signaling molecules as well as actin-binding proteins, actin microfilaments, and microtubules (Raftopoulou and Hall, 2004; Webb et al., 2004; Ezratty et al., 2005). Talin, a direct cytoplasmic β integrin–binding protein, is involved in adhesion site formation, reinforcement, and stabilization (Albiges-Rizo et al., 1995; Priddle et al., 1998; Giannone et al., 2003; Jiang et al., 2003) as well as in integrin activation and local PIP_2 generation (Martel et al., 2001; Calderwood et al., 2002; Tadokoro et al., 2003). Integrin clustering requires the formation of complexes composed of activated integrins, immobilized ligands, talin, and PIP_2 (Cluzel et al., 2005). Additionally, the calpain family regulates cell motility, partly by down-regulating integrin-mediated adhesion complexes (Bhatt et al., 2002) and through talin cleavage, a rate-limiting step during adhesion turnover, and is critical for FA disassembly (Franco et al., 2004). The current understanding is that integrin-containing adhesion sites function as signal transduction centers. Consequently, tight regulation of integrin affinity is crucial for adhesion signaling (Bennett, 2005). Integrins adopt high and low affinity conformations, and ligand–integrin binding is often preceded by intracellular changes, resulting in increased affinity (Ginsberg et al., 2005). Crystal structure analysis suggests a bent, hooklike conformation for the extracellular domain in the inactive state and an extended conformation in the active state (Liddington and Ginsberg, 2002; Takagi and Springer, 2002). Talin binding

Correspondence to Corinne Albiges-Rizo: corinne.albiges-rizo@ujf-grenoble.fr

Abbreviations used in this paper: FA, focal adhesion; FN, fibronectin; ICAP-1, integrin cytoplasmic domain–associated protein 1; MEF, mouse embryonic fibroblast; MFI, mean fluorescence intensity; VASP, vasodilator-stimulated phosphoprotein; VN, vitronectin; WT, wild type.

The online version of this article contains supplemental material.

The Journal of Cell Biology, Vol. 180, No. 2, January 28, 2008 427–441
http://www.jcb.org/cgi/doi/10.1083/jcb.200707142

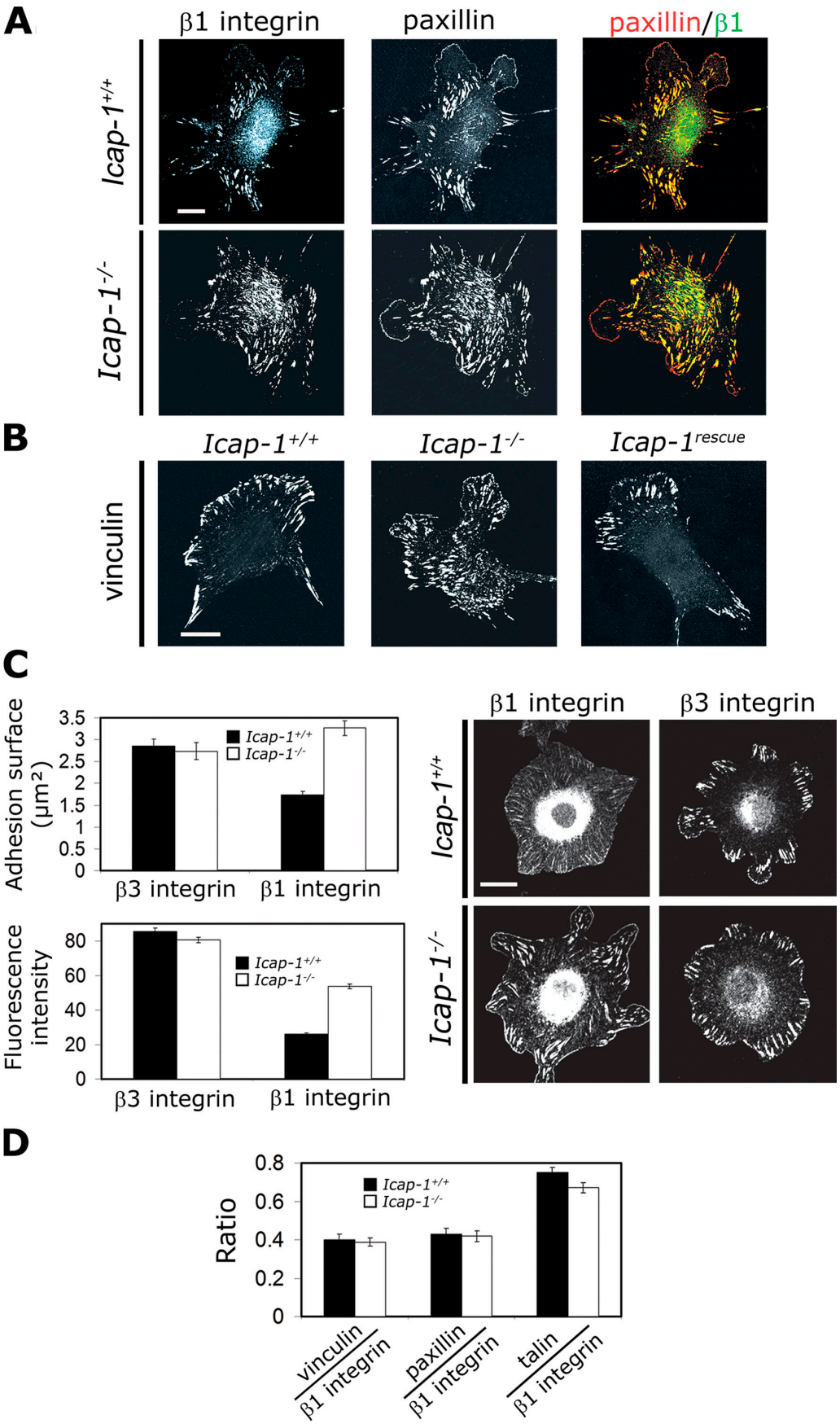

Figure 1. **ICAP-1 loss induces the central redistribution of FAs and increases β_1-integrin clustering.** (A and B) Confocal images obtained with *Icap-1*$^{+/+}$ and *Icap-1*$^{-/-}$ MEF cells (A) or *Icap-1*$^{+/+}$, *Icap-1*$^{-/-}$, and *Icap-1*^{rescue} osteoblasts (B). Cells were cultured overnight on 10 μg/ml FN and processed for

disrupts a salt bridge between the α and β subunits, leading to integrin activation (Luo et al., 2004; Vinogradova et al., 2004). Evidence suggests that the binding of a complex including talin, Rap1-GTP–interacting adaptor molecule, Rap1, and vasodilator-stimulated phosphoprotein (VASP) to the integrin cytoplasmic tail is a common final step in integrin activation (Han et al., 2006).

Among integrin partners, integrin cytoplasmic domain–associated protein 1 (ICAP-1) encompassing a phosphotyrosine-binding domain interacts specifically with the cytoplasmic tail of β_1 integrin at the membrane-distal NPXY motif. The increase of β_1 integrin–dependent cell motility on fibronectin (FN) upon ICAP-1 overexpression (Chang et al., 1997, 2002; Zhang and Hemler, 1999) and cell rounding up after overexpression of a phosphomimetic mutant of ICAP-1 at the CaMKII site (Bouvard and Block, 1998) suggest that ICAP-1 might regulate β_1-integrin function. Moreover, talin and ICAP-1 compete in vitro for integrin binding, and high ICAP-1 concentrations disrupt FA (Bouvard et al., 2003). ICAP-1 and β_1 integrin are colocalized at the leading edges of cells during the early stages of spreading (Fournier et al., 2002). This facet of ICAP-1 in FA dynamics, which is obviously regulatory and transitory, prompted us to determine in more detail the role played by ICAP-1 in adhesion site dynamics.

In this study, we show that *Icap-1*–deficient mouse embryonic fibroblasts (MEFs) display defects in cellular spreading and migration correlating with the redistribution of FA, a modification in FA dynamics, and an increase in integrin affinity. These defects could be mimicked by increasing either integrin affinity or the surface density of the underlying matrix. By modulating integrin affinity, ICAP-1 allows the cell to adapt its adhesion strength and rate of migration to changes in the matrix surface density. These data point not only to the existence of specific molecules involved in FA assembly or disassembly signaling pathways but also to the control of FA assembly and matrix sensing through the fine-tuning of integrin affinity.

Results

ICAP-1 loss alters the distribution and morphometry of FA

To figure out the role of ICAP-1 in FA dynamics, we compared the adhesive behavior of MEFs isolated from wild-type (WT) and *Icap-1*–deficient mice embryos as well as in WT, *Icap-1*–null, and *Icap-1* rescued osteoblasts. Immunostaining revealed paxillin- and β_1 integrin–containing FAs to be distributed throughout the ventral cell surface in *Icap-1*–null MEFs, whereas WT cells exhibited mostly peripheral FAs (Fig. 1 A). In contrast, distribution of the β_3 integrin (known not to interact with ICAP-1)–containing FA was not modified in *Icap-1*–null cells (Fig. S1 A, available at http://www.jcb.org/cgi/content/full/jcb.200707142/DC1). FA distribution defects were ICAP-1 dependent and not cell specific because centrally located FAs in *Icap-1*–null osteoblasts were redistributed peripherally after *Icap-1* rescue (Fig. 1 B). This altered FA distribution was also associated with a modification of their morphometry. β_1 integrin–containing FAs on FN were significantly larger in *Icap-1*–null fibroblasts, whereas the size of β_3 integrin–containing FAs remained identical for both cell types (Fig. 1 C). β_1-integrin clustering within FA, which was estimated by the mean fluorescence intensity (MFI), was increased by about twofold in *Icap-1*–null cells compared with WT cells (Fig. 1 C). Then, we analyzed the putative role of ICAP-1 in the regulation of FA composition (Fig. 1 D). Talin, vinculin, and paxillin as well as surface β_1 and β_3 integrins were expressed at similar levels in both cell types (Fig. S1, B and C). Constant adaptor protein/integrin ratios in both cell types indicates that ICAP-1 did not interfere with FA constitution and reveals that β_1 integrins highly clustered within FA in null cells are fully competent to bind their intracellular partners (Fig. 1 D). Thus, the increased size of FAs in *Icap-1*–null MEFs could be attributed to increased β_1-integrin clustering and not to an indirect change in adhesion protein expression or to a modification in the cell surface expression of β_3 and β_1 integrins.

Icap-1–null cells exhibit a shift in the optimum ECM surface density required for cell migration and spreading

As the modification in the FA pattern and morphometry reflects cell adhesion and migratory defects, we monitored the migration rate of MEFs spread on increasing concentrations of β_1 integrin–engaging matrices, FN and type I collagen (CL). The typical bell-shaped curve observed for WT cells was shifted toward the lower densities of ECM substrates for *Icap-1*–deficient cells. Indeed, the optimal matrix concentration required for the maximum migration of *Icap-1*–deficient cells was reduced 10-fold and 20-fold for FN and CL coatings, respectively (Fig. 2 A). A very similar result was obtained with FN using time-lapse video microscopy (Fig. 2 B).

Because migratory properties were modified in *Icap-1*–null MEFs, we investigated the consequences of ICAP-1 loss on cell spreading. The densities required to reach similar spreading levels on both matrices were much lower with *Icap-1*–null cells than with WT cells. Indeed, with FN, 50% spreading was achieved at a 0.5-μg/ml coating concentration for *Icap-1*–null cells versus 1 μg/ml for WT cells (Fig. 2 C). Similar results

immunofluorescence labeling to visualize β_1 integrin (9EG7), paxillin, and vinculin. Note the increased number of FAs at the cell surface underlying the main cell body in *Icap-1*$^{-/-}$ MEF cells and osteoblasts and the exclusive peripheral distribution of adhesion sites in rescued osteoblasts. (C and D) *Icap-1*$^{+/+}$ and *Icap-1*$^{-/-}$ MEF cells were plated on 10 μg/ml FN and allowed to spread for 2 h. Immunostaining was processed to visualize vinculin, paxillin, and β_1 or β_3 integrins. Confocal images of each cell type were acquired and subjected to image analysis with MetaMorph software. (C) The mean surface of β_3 or β_1 integrins containing FA (top histogram) and the MFI of β_1 and β_3 integrins in vinculin-stained FAs (bottom histogram) were measured in *Icap-1*$^{+/+}$ and *Icap-1*$^{-/-}$ MEF cells. Right images show β_1 and β_3 integrin–containing FAs in both cell types. (D) The ratio of the mean intensities of vinculin-, paxillin-, or talin-containing FAs normalized to β_1 integrin was then estimated. Experiments were performed in duplicate, and at least 20 cells were analyzed for each immunostaining. Error bars indicate SD. Bars, 20 μm.

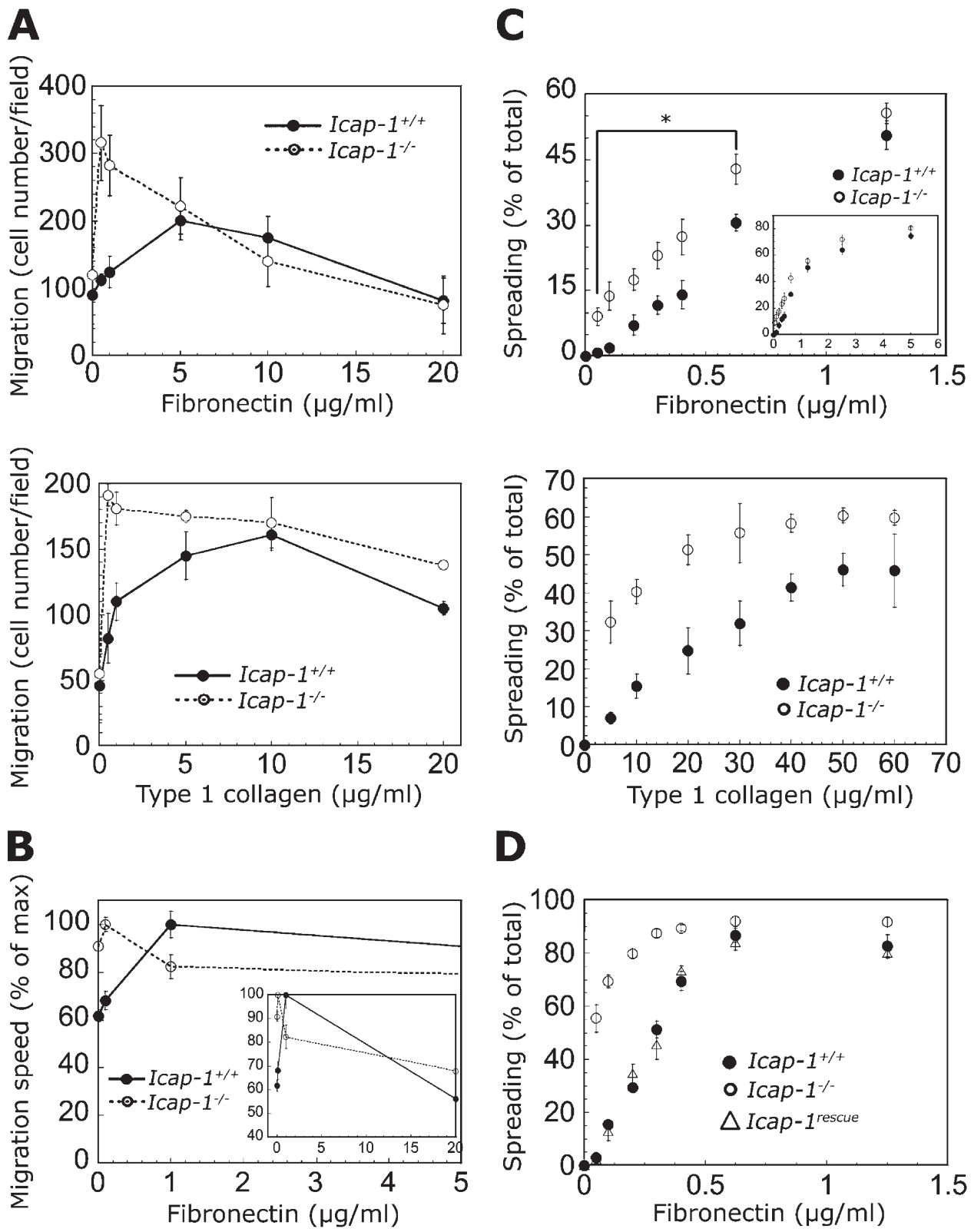

Figure 2. **ICAP-1 loss shifts the optimum substrate concentration for migration and facilitated adhesion.** (A) The migration of *Icap-1*$^{+/+}$ and *Icap-1*$^{-/-}$ MEF cells was studied in a random chemotactic transwell assay. Cells were seeded in transwell chambers coated on both sides with increasing concentrations of FN or CL ranging from 0.5 to 20 μg/ml. After 8 h, cell migration was stopped, and cells were stained and fixed by Coomassie blue. The cells localized on the underside of the membrane were counted, and the number of cells per field was used to quantify cell migration. (B) The migration speed of *Icap-1*$^{+/+}$ and *Icap-1*$^{-/-}$ MEF cells was determined on various FN concentrations by using time-lapse phase-contrast video microscopy and cell tracking with MetaMorph software. 20–40 cells were photographed for each experimental condition at 4-min intervals over an 8-h period. The maximal migration speed was used to set up 100% for each cell type. (A and B) Error bars indicate SD of at least thee individual experiments. (C and D) Spreading assay of *Icap-1*$^{+/+}$ and *Icap-1*$^{-/-}$ MEF cells (C) as well as *Icap-1*$^{+/+}$, *Icap-1*$^{-/-}$, and *Icap-1*^{rescue} osteoblasts (D) on increasing substrate densities. Cells were seeded

were obtained with CL: 50% spreading occurred at a coating concentration of 5 µg/ml for *Icap-1*–null cells compared with 25 µg/ml for WT cells (Fig. 2 C). *Icap-1*–null cells appeared to exhibit a stronger interaction with FN and CL and, consequently, spread at lower densities of these ECM substrates. In both migration and spreading assays, the differences between WT and mutant cells were more pronounced using CL. This probably reflects the more restricted use of β_1 integrins on CL. On the other hand, the expression of ICAP-1 in *Icap-1*–null MEFs restores cell spreading and migration similarly to what was observed for WT MEFs (Fig. S2, A and B; available at http://www.jcb.org/cgi/content/full/jcb.200707142/DC1), proving that the altered migration was indeed caused by the loss of endogenous ICAP-1. A similar effect was also observed with osteoblasts: at the FN-coating concentration of 0.3 µg/ml, the totality of *Icap-1*–null osteoblasts were fully spread, whereas only 50% of WT and rescued osteoblasts were spread under identical experimental conditions, demonstrating that this defect was still ICAP-1 dependent but not cell specific (Fig. 2 D). In agreement with the specificity of ICAP-1 for β_1 integrin, migration and adhesion behaviors of WT and *Icap-1*–null MEFs on vitronectin (VN) coating were not significantly different. This demonstrates that ICAP-1 loss did not alter β_3 integrin–mediated adhesion (Fig. S3, A and B).

ICAP-1 slows down the talin recruitment into FAs

The fact that *Icap-1*–null cells migrated and spread at lower matrix densities might reflect defects in adhesion dynamics. If ICAP-1 was involved in FA dynamics, differences are expected in the exchange or recruitment rate of some FA components between *Icap-1*–null cells and WT cells. To address this point, measurements of FRAP experiments were made using EGFP-fused vinculin or talin (Fig. 3). Single FA in the lamella was photobleached, and their fluorescence recovery was recorded. Recovery times (τ) were calculated for both fusion proteins. Our results revealed that EGFP-vinculin recruitment was four times faster than EGFP-talin in WT MEF cells spread on FN (Fig. 3 A). However, no difference between WT and *Icap-1*–deficient MEFs was observed in the incorporation speed of EGFP-vinculin into FAs, demonstrating that vinculin recruitment is ICAP-1 independent. Conversely, the recovery half-time associated with EGFP-talin was significantly lower in *Icap-1*–deficient MEFs, suggesting a faster recruitment of EGFP-talin in cells lacking ICAP-1. This conclusion is in line with the proposed competitive binding of ICAP-1 and talin for the β_1-integrin cytoplasmic domain (Bouvard et al., 2003). FRAP experiments were also performed in cells spread on β_3-integrin preferential substrate, such as VN to compare talin and vinculin recruitment in case of *Icap-1* deficiency (Fig. 3 B). As expected, no significant change in talin recruitment was observed in both cells spread on VN. Our results demonstrate that the function of ICAP-1 is dependent on adhesion on specific substrate.

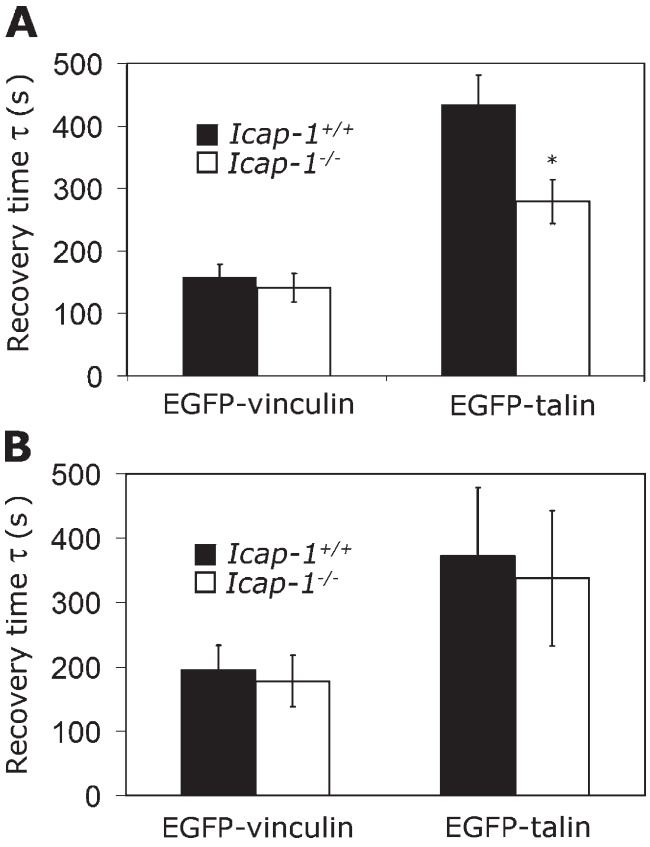

Figure 3. **ICAP-1 loss induces a faster recruitment of talin into FAs.** *Icap-1*$^{+/+}$ and *Icap-1*$^{-/-}$ MEF cells were seeded in LabTekII chambers coated with either 20 µg/ml FN (A) or 5 µg/ml VN (B) and were allowed to spread for 12 h. After transfection, both cell types expressing either EGFP-talin or EGFP-vinculin were subjected to FRAP experiments. Photobleaching was performed on manually delimited individual FAs localized at the edge of cells. EGFP fluorescence recovery was measured at 1-min intervals over a 15–20-min period, and the characteristic recovery time (τ) of each FA protein was estimated. At least 20 FAs were recorded for both cell types. Error bars indicate SD. The shorter recovery time, τ, of EGFP-talin in *Icap-1*$^{-/-}$ cells indicates a higher mobility of this protein (e.g., its faster recruitment into FA). *, $P \leq 0.01$.

ICAP-1 slows down FA assembly

Two key steps in cell migration are FA assembly and disassembly (Webb et al., 2004). To identify whether ICAP-1 was involved in FA turnover, WT and *Icap-1*–null MEF cells expressing EGFP-paxillin, EGFP-vinculin, or EGFP-VASP were monitored using time-lapse video microscopy over a 6-h period. Again, we noticed that EGFP-VASP (Fig. 4 A), EGFP-paxillin, or EGFP-vinculin (not depicted) expressed in *Icap-1*–null cells were mostly localized in central FAs. Cells were plated on a low concentration of FN (1 µg/ml) to promote cell migration. Turnover of FAs located at the leading edge were arbitrary decomposed into four parameters: namely, assembly (from the first appearance until the maximal pixel intensity level is reached), steady-state duration (no change of the maximal pixel intensity), disassembly rates (from the maximum pixel intensity is

on various concentrations of FN- or CL-coated surfaces and were allowed to spread for 1 h 30 min. Round and flattened cells were counted, and spread cells were expressed as the percentage of total cell number. The inset represents the same spreading assay with increasing concentrations of FN. Each data point represents the mean of at least three separate experiments, and error bars represent SD. *, $P \leq 0.03$.

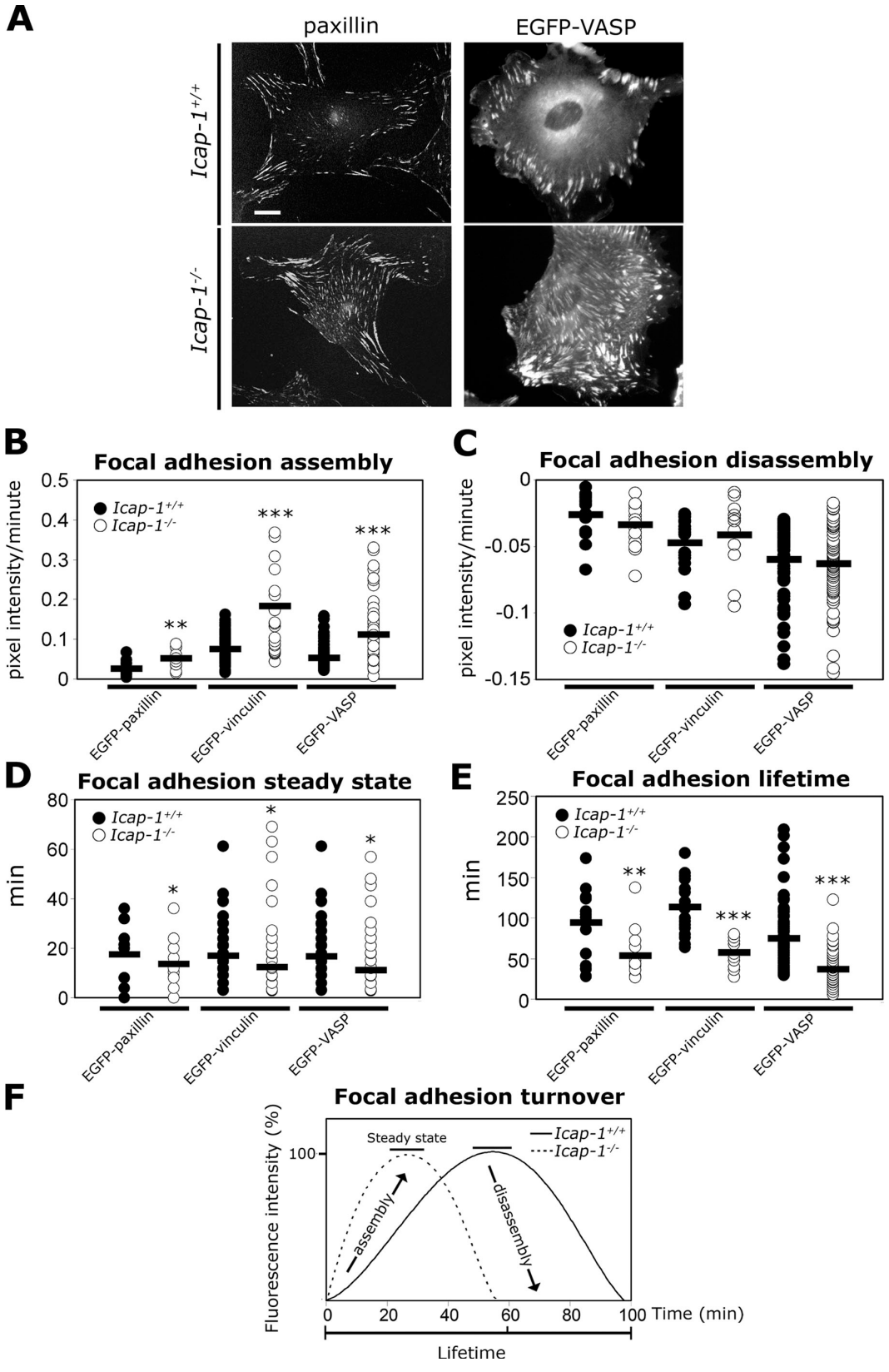

Figure 4. **ICAP-1 modulates FA turnover by controlling its assembly rate.** (A) Confocal images of *Icap-1*$^{+/+}$ and *Icap-1*$^{-/-}$ MEF cells either immunostained to visualize endogenous paxillin or transfected to express EGFP-VASP. (B–F) *Icap-1*$^{+/+}$ and *Icap-1*$^{-/-}$ MEF cells expressing either EGFP-paxillin, EGFP-vinculin, or EGFP-VASP were allowed to spread on 1 µg/ml FN for 12 h in a LabTekII chamber. Then, cells were imaged by time-lapse video microscopy at 4-min intervals for 6 h. The resulting data were subjected to image analysis using MetaMorph software. The mean pixel intensity of a defined FA was followed over time, and this analysis allowed the four parameters of FA turnover to be measured: measurement of the positive (B) or negative (C) variations per minute of the mean pixel intensity reflecting the assembly and disassembly rates, respectively, for each individual FA in *Icap-1*$^{+/+}$ and *Icap-1*$^{-/-}$ cells;

reached until FA is not resolvable), and total lifetime (from the first appearance of a resolvable FA until its disappearance). In *Icap-1*–null cells, the increase in EGFP-tagged protein intensity during FA assembly was significantly faster (Fig. 4, B and F), and the duration of the steady state was slightly shorter (Fig. 4 D) than for WT cells. In contrast, FA disassembly rates (Fig. 4, C and F) were identical for both cell types. These measurements showed that faster FA assembly associated with a minor reduction of the steady state upon ICAP-1 loss results in a shorter FA lifetime (Fig. 4, E and F). It is worth noting that this change in dynamics was not observed with *Icap-1*$^{-/-}$ cells spread on VN, thus underlining the action of ICAP-1 on β_1 integrins (Fig. S3 C). Altogether, these data suggest that ICAP-1 down-regulates cell migration and spreading by slowing down FA assembly involving β_1 integrins.

ICAP-1 is not required for FA disassembly

Previous work has highlighted an important role for microtubule networks in FA turnover (Kaverina et al., 1999; Ezratty et al., 2005). This is based on the finding that microtubule depolymerization upon nocodazole treatment increases FA assembly, whereas microtubule regrowth after nocodazole washout induces a rapid and reversible disassembly of FA. We took advantage of the synchronized disassembly of FAs induced by nocodazole to investigate the involvement of ICAP-1 in the control of this process. After 4 h of nocodazole treatment, the microtubule network totally collapsed, and WT MEFs displayed larger peripheral FAs (Fig. 5, A and B). However, *Icap-1*–deficient MEFs showed a dramatic increase in the number of central FAs, whereas the number and size of peripheral FAs were not significantly changed (Fig. 5, A and B). For both cell types, 60 min after nocodazole washout, FA disassembly temporally coincided with de novo growth of microtubules toward the cell periphery. FA reappeared 90 min after nocodazole washout, showing that FA disassembly was reversible in both cell types. Quantification of our observations revealed that nocodazole treatment of *Icap-1*–null cells induced the de novo formation of central but not peripheral FAs. In contrast, WT MEFs behaved differently because nocodazole induced a reinforcement of existing peripheral FAs without promoting de novo assembly (Fig. 5 B). Along with the video microscopy experiments, these results consistently suggested that ICAP-1 loss favored FA assembly but had no influence on disassembly.

Increased integrin affinity in *Icap-1*–deficient cells is responsible for the cell adhesion phenotype

As ICAP-1 competes with talin for β_1 cytoplasmic domain binding (Bouvard et al., 2003, 2007), the promotion of FA assembly resulting in the modification in migration and spreading of *Icap-1*–null fibroblasts could arise from an increase in β_1-integrin affinity. Indeed, the activation state of β_1 integrins measured by FACS revealed a higher affinity state in *Icap-1*–null cells than in WT cells (Fig. 6 A). This result is consistent with our recent work showing an increase in $\alpha_5\beta_1$-integrin affinity in osteoblasts issuing from *Icap-1*–null mice (Bouvard et al., 2007) and also suggests that this integrin affinity increase is cell type independent. To correlate the increase in β_1-integrin affinity to the adhesive defect observed in *Icap-1*–null cells, integrins were chemically activated in WT cells to mimic the *Icap-1*–null phenotype (Fig. 6, B and C; and Fig. S4, available at http://www.jcb.org/cgi/content/full/jcb.200707142/DC1). Mn^{2+} treatment of both WT and rescued cell types shifted the spreading curve toward lower FN or CL surface densities, whereas it had no effect on Mn^{2+}-treated *Icap-1*–null cells because their integrins are already in a high affinity state (Figs. 6 B and S4, A and B). These results were also confirmed with 9EG7 mAb, which is able to both recognize an activated β_1 integrin–specific epitope and maintain it in its high affinity conformation (Figs. 6 C and S4 C). Thus, it was tempting to speculate that β_1-integrin affinity could also control FA assembly. To test this hypothesis, we generated the activated β_1-integrin mutant D759A with a disrupted salt bridge between α and β subunits (Hughes et al., 1996; Sakai et al., 1998; Partridge et al., 2005) and expressed it in β_1 integrin–deficient GD25 cells. First, we confirmed that GD25/β_1D759A cells displayed a higher affinity for the FNIII7-10 fragment than GD25/β_1WT cells (Fig. 7 A). At moderate FN surface densities, FAs were centrally distributed in GD25/β_1D759A cells, whereas they were located on the periphery in control cells (Fig. 7 B). Both adhesive and migratory curves displayed a shift toward the lower matrix densities in mutant cells (Fig. 7 C). The coating concentration of FN giving the highest migration speed was approximately five times lower for GD25/β_1D759A cells. Mn^{2+} treatment of GD25/β_1WT integrin cells induced a shift in the spreading curve and mimicked the adhesive behavior of GD25/β_1D759A and *Icap-1*–null cells. Finally, GD25/β_1D759A cells displayed a faster rate of FA assembly, which is associated with a shorter lifetime, without any significant modification in the duration of the steady state or the disassembly rate (Fig. 7 D). Altogether, these results suggest that the adhesive defect in *Icap-1*–null cells was the result of the presence of β_1 integrin in its active state and further implicate β_1-integrin activation in the regulation of FA assembly.

Control of β_1-integrin affinity by ICAP-1 allows ECM density sensing

The reduced amount of adsorbed matrix required to support cell migration or spreading observed for *Icap-1*–null cells suggests that the sensing of matrix surface density has been changed. Moreover, the activation of β_1 integrin displaces the maximal

the time during which the mean pixel intensity did not fluctuate corresponds to the FA steady state (D); and the total time during which EGFP-fused adhesion proteins remain localized in a FA represents the FA lifetime (E). At least 20 cells of both cell types were recorded. Each point represents an individual FA, and the horizontal bars are the mean of all FAs. (F) These four parameters were compiled in a schematic model of FA turnover in *Icap-1*$^{+/+}$ and *Icap-1*$^{-/-}$ cells. The higher FA assembly rate in *Icap-1*$^{-/-}$ cells and the reduced steady-state duration induced the shortening of FA lifetime. *, $P < 0.05$; **, $P < 10^4$; ***, $P < 10^6$. Bar, 20 µm.

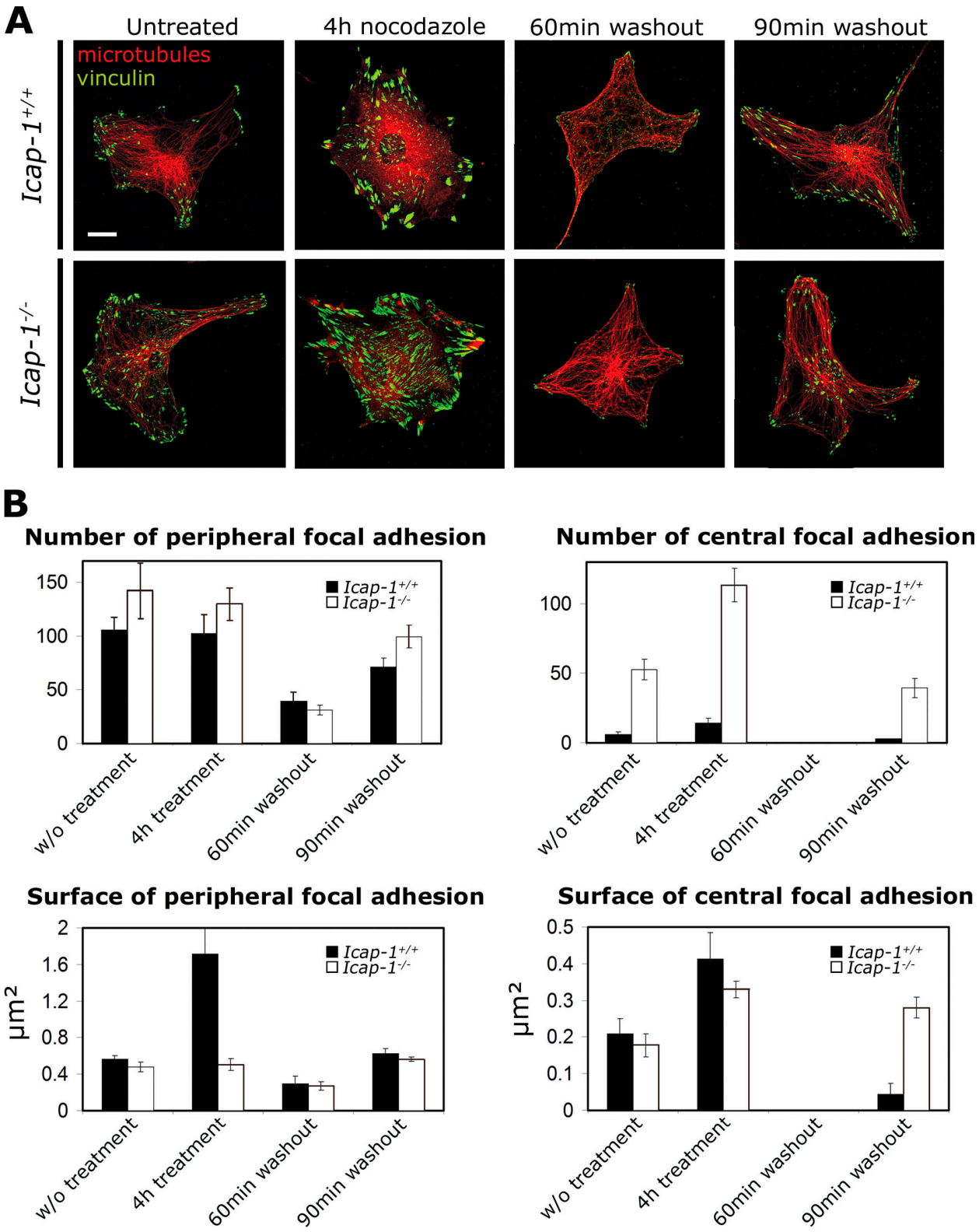

Figure 5. **ICAP-1 loss induces de novo FA formation upon nocodazole treatment.** (A) *Icap-1*$^{+/+}$ and *Icap-1*$^{-/-}$ MEF cells were either untreated or treated with 10 µM nocodazole for 4 h or treated with 10 µM nocodazole for 4 h followed by the drug washout for 60 and 90 min and were fixed. FA and microtubules were visualized by immunostaining of vinculin (green) and tyrosinated tubulin (red) and imaged using confocal microscopy. (B) Image quantification of vinculin-stained *Icap-1*$^{+/+}$ and *Icap-1*$^{-/-}$ cells. Peripheral (left) or central (right) FA number per cell was counted (top) at each indicated step of the nocodazole assay, and the corresponding mean surface (bottom) was quantified. 20 cells were analyzed for each experimental condition, and error bars indicate SD. Bar, 20 µm.

adhesive response to a significantly lower matrix concentration, suggesting that ICAP-1 is involved in the cell's perception and response to its microenvironment. We hypothesized that increasing substrate density would affect adhesion strength and favor the active state of the integrin. Indeed, WT MEFs on low density matrices showed only peripheral FAs (Fig. 8 A). At high matrix density, the observed increase in FA number distributed throughout the ventral cell surface was correlated with an increase in activated β_1-integrin recruitment into FAs (Fig. 8, B and C). However, in *Icap-1*–null MEFs, FAs were mostly distributed all over the ventral face regardless of the matrix density used. These results reveal that increasing substrate density induces β_1 integrin to take up its high affinity state and, furthermore, that ICAP-1 loss renders cells unable to sense the state of the matrix and adapt to variations in ECM density.

To assess whether the reduction in the adhesive response of *Icap-1*–null cells to matrix density could be attributed to some differential adhesion dynamics, we quantified FA turnover in cells at different FN matrix densities using time-lapse video microscopy (Fig. 8 D). In WT cells, increased matrix density (10–50 µg/ml) induced faster FA assembly. A similar effect was observed using *Icap-1*–null cells but at lower FN-coating densities. This result supported our hypothesis that matrix density affects FA assembly and that *Icap-1*–null cells can only poorly adapt their adhesive structures to increase in ECM density because of their already high adhesion strength at low matrix density. However, we noticed a rise in the length of the steady-state phase at higher matrix densities in both WT and null cells, suggesting that the control of FA dynamics during the stages after assembly is ICAP-1 independent but matrix density dependent. These results highlight the involvement of ICAP-1 in sensing the state of the matrix through control of FA assembly, thus enabling the cell to adapt its adhesive response to changes in properties of the ECM.

Discussion

In this study, we have used both *Icap-1*–deficient MEFs and active β_1-integrin mutants to show that the regulation of integrin affinity is necessary for the control of FA assembly and, consequently, also for cell spreading and cell migration. Our data demonstrate that ICAP-1 slows down FA assembly by decreasing β_1-integrin affinity. We also document a new and unexpected role for ICAP-1 in the regulation of integrin affinity for a proper matrix surface density sensing. Therefore, ICAP-1 belongs to the molecular machinery of the FA that is able to provide the cell with the ability to respond adaptively to changes in substrate density.

Our present work provides an array of convergent clues in support of a critical role for ICAP-1 in the control of FA turnover. Indeed, the faster assembly rate of FA in the lamella of *Icap-1*–null cells accelerates the maturation state of the adhesion and is associated with a slightly shorter steady state, resulting in a reduced lifetime. However, as the rate of FA disassembly is not modified by the lack of ICAP-1, this strongly suggests that disassembly is triggered by an ICAP-1–independent signaling pathway. Although some proteins such as paxillin and FAK

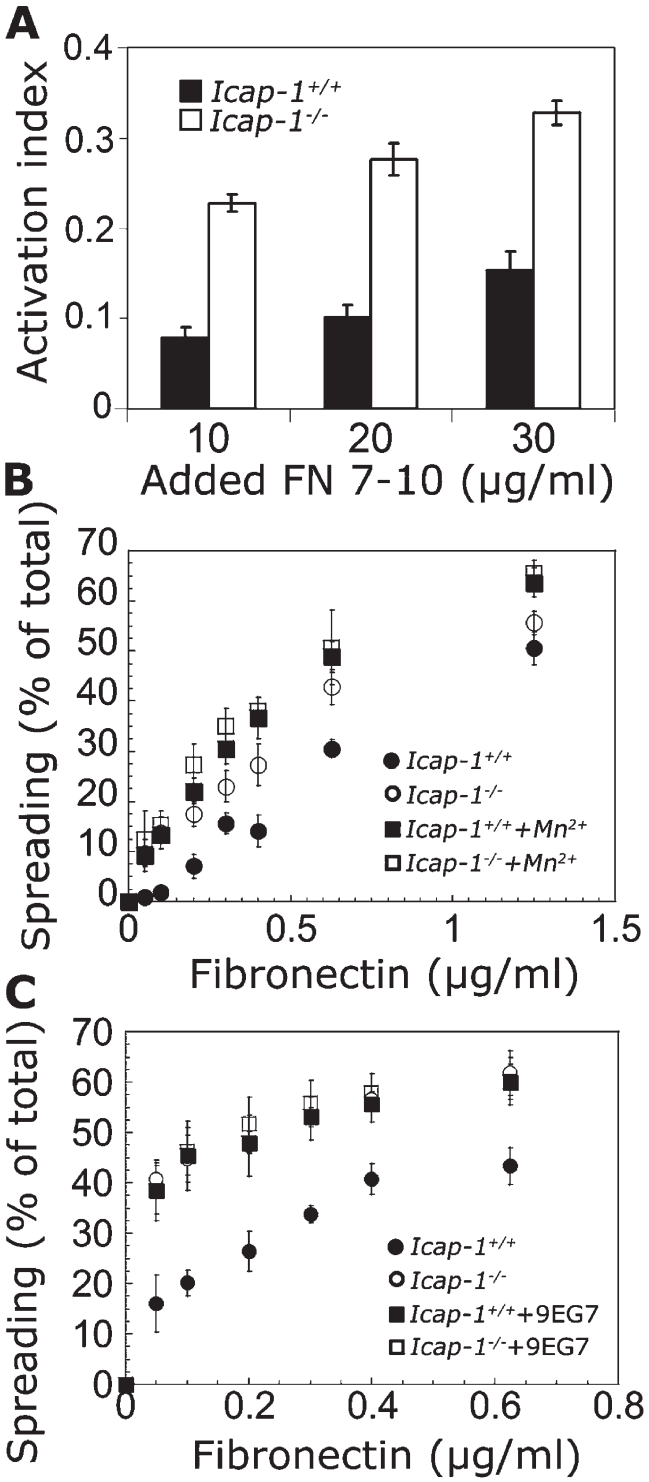

Figure 6. **β_1-integrin activation induces a spreading phenotype similar to ICAP-1 loss.** (A) The β_1-integrin activation state in *Icap-1*$^{+/+}$ and *Icap-1*$^{-/-}$ cells was determined by an FNIII7-10 binding assay that measures the ability of integrins to bind FITC-conjugated FNIII7-10 by flow cytometry analysis as described in Materials and methods. The activation index of integrin was expressed relative to the cell surface expression of β_1 integrin as previously estimated by flow cytometry using MB1.2 mAb. (B and C) Spreading assays of *Icap-1*$^{+/+}$ and *Icap-1*$^{-/-}$ MEF cells with or without treatment using either 0.5 mM $MnCl_2$ (B) or with 10 µg/ml 9EG7 mAb (C). Cells were first treated in suspension and were plated in a dose-dependent manner on FN. Cell spreading was measured as described in Fig. 2 C. Error bars indicate SD from three independent experiments.

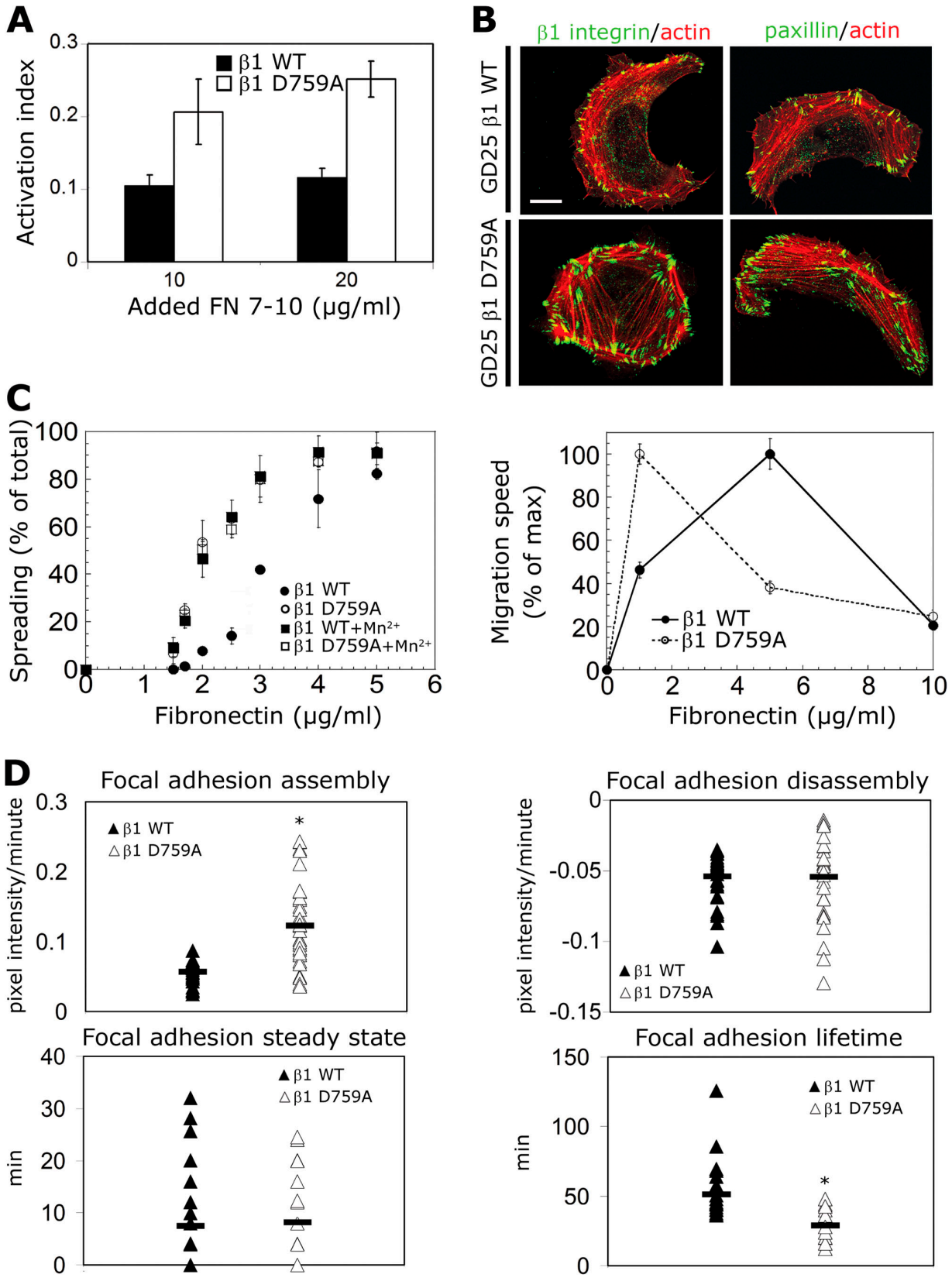

Figure 7. **Activated β_1 integrin increases FA turnover and promotes cell migration and spreading at low matrix density.** The human WT β_1-integrin chains or activated mutant (D759A) were stably expressed in β_1 integrin–deficient GD25 cells, and their adhesive properties were analyzed. (A) The integrin affinity state for both cell types was measured with the FNIII7-10 binding assay as described in Fig. 6 A. (B) Confocal images of GD25/WT and D759A β_1 cells spread on 10 μg/ml FN and immunostained to visualize β_1 integrin, paxillin, and filamentous actin. β_1 integrin was labeled with the 4B7R mAb, which recognizes the human β_1-integrin chain. (C) Cell spreading and migration assays of GD25/WT and D759A β_1 cells. Spreading of both cells types with or without 0.5 mM $MnCl_2$ treatment was measured as described in Fig. 6 B. Migration of both cells types was analyzed using time-lapse phase-contrast video

are involved in FA disassembly (Webb et al., 2004; Schober et al., 2007; Zaidel-Bar et al., 2007), to date, ICAP-1 is the only regulatory molecule shown so far to negatively control the assembly phase. The specific interaction of ICAP-1 with the β_1 integrins (Chang et al., 1997) combined with the change in the adhesion properties of *Icap-1*–null cells, depending on the integrin-engaging substrates, indicate that the observed modification in FA dynamics in these cells probably involves the participation of β_1 integrins.

Modification in the dynamics of β_1 integrin–containing FAs in *Icap-1*–null cells is also revealed by the faster recruitment of EGFP-talin into FAs observed by FRAP studies. This observation in living cells fits with in vitro talin–ICAP-1 competition assays as well as with the FA disruption and cell rounding up occurring after ICAP-1 overexpression. Although FRAP experiment could not definitively measure the increase of the on-rate of talin into FA, these results support the idea that ICAP-1 competes with talin for binding to the β_1 cytosolic tail (Bouvard and Block, 1998; Bouvard et al., 2003). We propose that ICAP-1 can delay the talin–integrin interaction necessary for integrin activation and clustering (Giannone et al., 2003; Calderwood, 2004; Cluzel et al., 2005). This also suggests that by modulating talin–integrin interaction, ICAP-1 could limit the incorporation of β_1 integrins into FAs, resulting in a modification in FA dynamics. However, we cannot exclude that the faster recruitment of talin into FA in *Icap-1*–null cells could be correlated with increased FAK or Src signaling in the β_1 integrin–enriched FA. This could also indicate an alteration in the affinity of talin for β_1 integrin, resulting in the overall instability of FAs and their faster FA turnover. Our FACS analysis of fluorescent FNIII7-10 binding on cells in suspension show that the loss of ICAP-1 increases the affinity of integrin for the ligand, although not as much as is achieved by incubation with either with Mn^{2+} or 9EG7 antibody. This favors the hypothesis whereby ICAP-1 limits a state of preactivation necessary for the following steps of activation. Without ICAP-1, this limitation is switched off, which, in turn, accelerates cellular mechanisms such as spreading or migration. Interestingly, when cells spread or migrate, any means of integrin activation (D/A, ICAP-1 loss, or chemical treatment) results in the same phenotype. This fits with our observation that D/A and *Icap-1*–null cells share the same phenotype but also suggests that either a threshold in integrin activation exists or that integrin activation is tightly controlled in space and time by a multistep process, implying different integrin states from preactivation to full activation of integrin as already suggested (Clark et al., 2005). Moreover, FA distribution in the cell central region is cell type specific because β_1 integrin–deficient osteoblasts infected with D759A human β_1 integrin display more FA in the cell central region compared with GD25/β_1D759A cells (unpublished data).

Although the control of the β_1-integrin high affinity state has been well characterized and is largely attributed to the interaction with talin (Calderwood, 2004), the mechanisms restricting β_1 integrin in a low affinity state are still unknown. Here, we show that ICAP-1 loss results in increased β_1-integrin affinity in MEFs, as previously described for osteoblasts (Bouvard et al., 2007). Importantly, this increase of β_1-integrin affinity in *Icap-1*–null cells results in faster FA turnover and in the inability of the cells to adapt their adhesive properties. This abnormal switch of β_1 integrins toward the high affinity state results in maximal cell spreading and migratory response on a coating of minimal substrate density even though no migration defect has been noticed in *Icap-1*–null mice during embryogenesis. Nevertheless, we can neither exclude the presence of a more subtle defect nor exclude the possibility of a migration defect in *Icap-1*–null mice during repair or pathogenesis. Mice expressing a D759A mutation in β_1 locus have been recently described (Czuchra et al., 2006). In contrast to *Icap*-1–null mice, those animals do not display significant abnormalities (Czuchra et al., 2006). However, although talin binding onto β_1 integrin is required for its full activation in both mutants, the absence of ICAP-1 expression would favor talin binding, whereas ICAP-1 would still limit this step in the case of the D/A mutation. It is also important to note the discrepancy of adhesive phenotype between keratinocytes isolated from D/A mice (Czuchra et al., 2006) and *Icap-1*–null cells, which could arise from the different integrin repertoires between mesenchymal cells (MEFs or osteoblasts) and epithelial cells (keratinocytes). Furthermore, *Icap-1*–deficient mice also suffer from a strong osteoblast proliferation defect that could be integrin independent (Bouvard et al., 2007).

However, our results indicate that a balance between low and high affinity integrin states is necessary for proper sensing of the ECM density, which, in turn, has important consequences for migration and spreading. Cell adhesion is continually adapted in response to changes in substrate concentration and structure or to mechanical cues at the cell–matrix interface. Distinct FA and actin cytoskeleton organization and dynamics have been shown to depend on the strength of cell adhesion (Gupton and Waterman-Storer, 2006). Our data provide new insight by adding integrin affinity regulation to the molecular mechanisms controlling these different processes. Change in adhesive properties can be predicted on the basis of the redistribution of FA. In our study, the hallmark of increased integrin affinity, corresponding to the signature of cellular adaptation to a particular matrix environment, is the redistribution of FA throughout the ventral cell surface accompanied by an expansion in their areas. These central FAs do not display the characteristics of fibrillar adhesions and are not correlated with an increased capacity to deposit FN matrix (unpublished data). Cells lacking ICAP-1 are much less capable of sensing different matrix densities; consequently, maximal response is elicited by a minimum matrix

microscopy and cell tracking as described in Fig. 2 B. (D) GD25 cells stably expressing EGFP-zyxin and either WT β_1 or D759A integrin were spread on 5 µg/ml FN and monitored by time-lapse video microscopy at 4-min intervals for 6 h. FA dynamics were assessed as described in Fig. 4. Four parameters for FA located at the leading edge of migrating cells were measured: assembly and disassembly speed, steady-state duration, and lifetime. Horizontal bars are the mean of all FAs. Error bars indicate SD. *, $P < 10^5$. Bar, 20 µm.

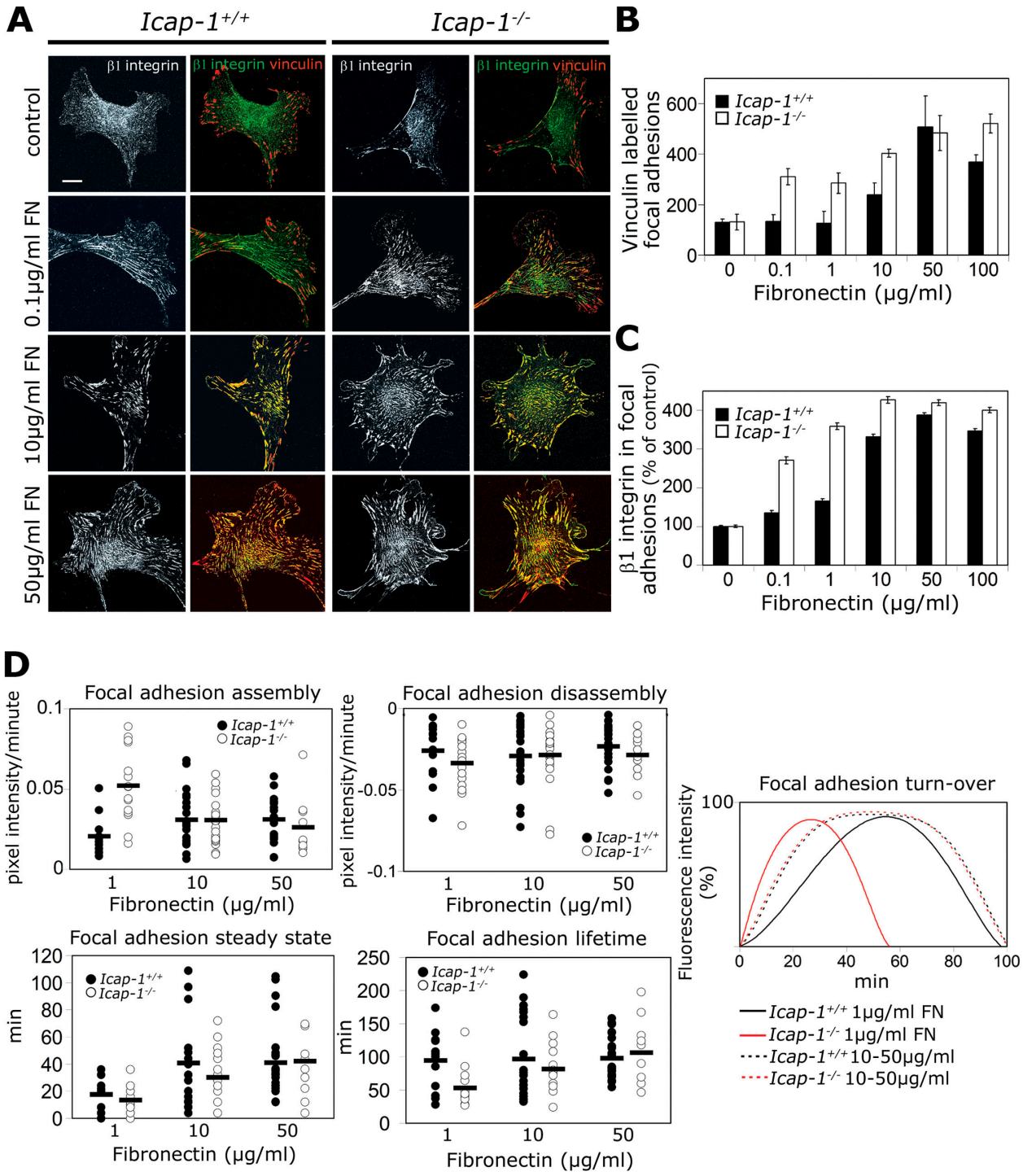

Figure 8. **ICAP-1 loss decreases matrix density sensing.** (A) *Icap-1*$^{+/+}$ and *Icap-1*$^{-/-}$ MEF cells were allowed to spread on glass coverslips coated or not coated (control) with increased FN concentrations in FCS-containing medium and were immunostained to visualize vinculin and β_1 integrin (9EG7). Images were taken with a confocal microscope. (B and C) The number of vinculin-stained FAs/cell (B) and the MFI of β_1-integrin staining within FAs (C) were measured for each FN concentration. 50 cells were analyzed for each experimental condition, and error bars indicate SD. (D) EGFP-paxillin–expressing *Icap-1*$^{+/+}$ and *Icap-1*$^{-/-}$ MEF cells were spread on FN at concentrations ranging from 1 to 50 µg/ml and were recorded by time-lapse video microscopy at 4-min intervals for 6 h. FA turnover was quantified as previously described in Fig. 4: the rates of FA assembly and disassembly were determined as well as the duration of the steady state and total lifetime at three different FN densities (1, 10, and 50 µg/ml). Data from at least 20 cells per experimental condition were recorded. Each point represents a single FA, and the horizontal bars show the means of all FAs. These parameters were compiled in a schematic model of FA turnover in *Icap-1*$^{+/+}$ and *Icap-1*$^{-/-}$ cells. Adhesion site turnover displays different behaviors depending on matrix density. Note the appearance of a steady-state plateau in both cell types at high FN concentrations without any change in FA lifetime. Error bars represent SD. Bar, 20 µm.

density environment. Cell adaptive response and stem cell lineage specification may arise from substrate stiffness (Discher et al., 2005; Paszek et al., 2005; Engler et al., 2006). This inability to feel their environment has important consequences for in vivo function. Indeed, *Icap-1*–null mice suffer from an important osteogenesis dysfunction resulting from reduced proliferation and delayed differentiation of the osteoblast population. *Icap-1*–deficient preosteoblasts present a condensation defect that further limits the number of progenitors that will finally differentiate into mature osteoblasts (Bouvard et al., 2007). This cell compaction defect could be a consequence of the cells' inability to sense the matrix density or organization. The pronounced phenotype in osteoblasts may be caused by their extraordinary need for mechanosensitivity to mediate bone formation and remodeling along with the necessity of being aware of the inherent variability in cellular response to differences in matrix density or stiffness (Leucht et al., 2007). Although it is clear from previous work that β_1-integrin expression is crucial for development and tissue homeostasis, we clearly establish that a switch between high and low affinity integrin states is required to drive an integrated cell response that is appropriate for the ECM environment. This is achieved by specific integrin regulators such as talin, ICAP-1, and possibly other proteins that are central to the control of FA dynamics during cell adhesion.

Materials and methods

Reagents and antibodies

FN was extracted from human plasma (Albiges-Rizo et al., 1995). Rat CL was purchased from Roche, and VN was purchased from Becton Dickinson. Vinculin mAb (hVIN-1), actin pAb (AC40), talin mAb (8d4), and phalloidin-rhodamine were obtained from Sigma-Aldrich. Paxillin mAb (349) was purchased from BD Biosciences. Anti–human β_1-integrin mAb (4B7R) was obtained from Lab Vision Corp. Anti–mouse β_1-integrin 9EG7 and MB1.2 mAb were obtained from BD Biosciences and provided by M.C. Bosco (University of Western Ontario, Ontario, Canada), respectively. Anti–mouse β_3-integrin mAb was provided by B. Nieswandt (Rudolf Virchow Center, University of Würzburg, Würzburg, Germany). Tyrosinated tubulin pAb was provided by L. Lafenachère (Unité Mixte de Recherche 5168, Grenoble, France). AlexaFluor-conjugated goat antibodies were purchased from Invitrogen. Rabbit anti–ICAP-1 serum was raised by immunizing rabbits with purified recombinant His-tagged ICAP-1 (amino acids 1–150) as antigen. Goat anti–mouse IgG and goat anti–rabbit IgG coupled to HRP were purchased from Bio-Rad Laboratories and Jackson ImmunoResearch Laboratories, respectively.

Cell culture, transfection, retroviral infection, and plasmid construction

Primary MEFs were isolated from embryonic day 14.5 WT or *Icap-1*–deficient embryos using a standard procedure. Immortalized osteoblasts from *Icap-1*$^{+/+}$ and *Icap-1*–null mice as well as *Icap-1*–null osteoblasts rescued with *Icap-1* were generated as described previously (Bouvard et al., 2007). MEF, GD25, and osteoblast cells were cultured in DME supplemented with 10% FCS (Invitrogen) and 100 U/ml penicillin/100 µg/ml streptomycin at 37°C in a 5% CO_2-humidified chamber. Cells were transfected with the cDNA constructs using ExGen 500 (Euromedex). The expression vectors were pEGFP-C1-vinculin, pEGFP-C1-paxillin (provided by K. Nakamura, Osaka Bioscience Institute, Osaka, Japan), pEGFP-C1-talin (provided by A. Huttenlocher, University of Wisconsin, Madison, WI), pBabe β_1-WT, pBabe β_1(D759A), pBabe-EGFP-VASP (provided by F. Gertler, Massachusetts Institute of Technology, Cambridge, MA), and pCLMFG-IRES–ICAP-1. Retroviral plasmid encoding human WT β_1 integrin or the D759A mutant was performed using standard protocols. In brief, a HindIII subclone fragment was used for PCR-mediated mutagenesis using the QuikChange Site-Directed Mutagenesis kit (Stratagene) according to the manufacturer's instructions and was reinserted into the full sequence to swap the WT sequence using HindIII digest. Human WT or mutant β_1 integrin was then inserted into the pBabe retroviral vector using EcoRI and XhoI sites. All sequences were verified by DNA sequencing (Genome Express). β_1 Integrin–null GD25 cells were transfected with pBabe containing either WT or D759A β_1 integrin and were selected in the presence of 1 µg/ml puromycin. For retroviral infection, cells were incubated for 24 h at 37°C with either pBabe-EGFP-VASP, pCLMFG-Ires–ICAP-1, or pCLMFG-EGFP-zyxin retrovirus containing supernant in 10% FCS-DME and 4 µg/ml Polybrene (Sigma Aldrich) as previously described (Bouvard et al., 2007).

Western blotting

MEF cells were lysed in radioimmunoprecipitation assay buffer containing protease and phosphatase inhibitors (Roche). Proteins were separated by SDS-PAGE and transferred to polyvinylidene difluoride membranes. Immunological detection was achieved with appropriate HRP-conjugated secondary antibody. Peroxidase activity was visualized by chemiluminescence (ECL; GE Healthcare).

Immunofluorescence staining of cells

Cells were fixed with 4% PFA, permeabilized with 0.2% Triton X-100, and incubated with appropriate primary antibodies. After rinsing, coverslips were incubated with an appropriate AlexaFluor-conjugated secondary antibody. The cells were mounted in Mowiol/DAPI solution and imaged on an inverted confocal microscope (LSM510; Carl Zeiss, Inc.).

Spreading assays

Cell adhesion assays were performed using 35-mm-diameter hydrophobic dishes coated with various concentrations of matrix. Cells were trypsinized, treated with 1 mg/ml trypsin inhibitor (Sigma-Aldrich), and incubated in serum-free DME/5% BSA for 1 h at 37°C. Cells were plated at a density of 2×10^4 cells per dish in 2 ml DME containing FN-free 10% FCS. After 1.5 h of incubation at 37°C, cells were photographed and scored as round or flattened using three fields for each experimental condition. When Mn^{2+} was supplemented, cells were treated for 10 min at 37°C in suspension with 0.5 mM $MnCl_2$ in DME containing FN-free FCS before seeding. Alternatively, cells were treated with 10 µg/ml mAb(9EG7) for 30 min at 4°C in DME containing FN-free FCS.

Migration assays

For transwell assays, polycarbonate membranes (8-µm pores; BD Biosciences) were coated on both sides overnight with various concentrations of matrix. After washing with PBS, chambers were transferred in 24-well plates containing either serum-free DME or DME plus FN-free serum. Serum-starved cells were trypsinized and treated with trypsin inhibitor. 15×10^3 cells were seeded in the upper chamber in 1 ml of serum-free DME and allowed to migrate to the underside of the membrane for 8 h. Cell migration was stopped by fixing and staining with Coomassie blue. Excess dye was removed with isopropanol/acetic acid. After removal of the nonmigrating cells in the upper well, migrating cells were photographed at 10× magnification and counted using three randomly chosen microscopic fields.

Time-lapse video microscopy was performed using chambered coverglass (LabTekII; Thermo Fisher Scientific) coated with various concentrations of FN. Trypsinized cells were treated with trypsin inhibitor and incubated in 5% BSA for 1 h at 37°C. Cells were then plated in LabTekII chambers containing DME supplemented with FN-free serum. After 1 h of spreading, cells were observed at 10× magnification using an inverted microscope (Axiovert 100; Carl Zeiss, Inc.) equipped with an on-stage incubator (XL-3; PeCon). Six to eight isolated fields were arbitrary chosen, and phase-contrast images were taken at 4-min intervals over a period of 5 h. Cells were tracked using the position of centroids with MetaMorph software (Roper Scientific).

FNIII7-10 binding assay and flow cytometry analysis

MEF or GD25 cells were harvested after trypsin treatment, washed in the presence of trypsin inhibitor, and incubated (3×10^5 cells per sample) with 3 µM FITC-coupled FNIII7-10 fragment (provided by F. Coussin, Unité Mixte de Recherche 5017, Bordeaux, France) in Tyrode buffer supplemented with 1% BSA for 1 h in the presence or absence of 5 mM EDTA and 5 mM EGTA. After washing with Tyrode/BSA, the cells were fixed and subjected to flow cytometry analysis using a FACScan flow cytometer (BD Biosciences). The collected data were analyzed using CellQuest software (BD Biosciences). In parallel, MEF or GD25 cells were analyzed by FACS for cell surface β_1- or β_3-integrin expression using either the MB1.2 rat mAb (against mouse β_1 integrin), the 4B7R mouse mAb (against human β_1 integrin), or the anti–mouse β_3-integrin rat mAb (against mouse β_3 integrin). The activation index of β_1 integrin was estimated as previously described (Bouvard et al., 2007). Each specific MFI was calculated by subtracting the background obtained with FnIII7-10 fragment incubation in the presence of EDTA or without the primary antibody in the case of the integrin labeling.

For instance, for the estimation of human β_1-integrin activation (GD25 cells), activation index = ([MFI FnIII7-10]−[MFI FnIII7-10 + EDTA])/([MFI 4B7R]−[MFI 4B7R control]).

Nocodazole assay

Cells were serum starved for 48 h in DME containing 0.5% fatty acid–free BSA and were treated with 10 μM nocodazole for 4 h to completely depolymerize microtubules. The drug was washed out with serum-free DME medium containing 0.5% fatty acid–free BSA, and microtubules were allowed to repolymerize for different time intervals. Cells were fixed and permeabilized before processing for immunofluorescence.

Quantification of FA area and intensity

Fixed and stained cells were imaged on a nonlinear optics LSM510 inverted confocal and biphoton laser-scanning microscope equipped with a 63× NA 1.4 oil-immersion plan Apochromat objective (Carl Zeiss, Inc.). The fluorescence of AlexaFluor488 and 546 was excited with 488- or 543-nm wavelengths and detected in confocal mode. AlexaFluor350 fluorescence was induced by two-photon absorption at 720 nm using the fs Ti-Sa laser (Tsunami; Spectra-Physics). Neither signal saturation nor significant photobleaching was induced during image acquisition in either detection channel.

The images were manually thresholded, and FAs were automatically selected using MetaMorph software within the predefined regions of the cell. The number and areas of FAs and the MFIs of β_1, β_3 integrin, vinculin, and paxillin in FAs were quantified.

Time-lapse video microscopy and quantification of FA dynamics

Time-lapse recordings were assessed either on MEF cells expressing EGFP-paxillin, EGFP-VASP, or EGFP-vinculin and on GD25 cells expressing EGFP-zyxin. Cells were cultured in FN-free FCS-DME on LabTekII chambers previously coated with the indicated concentrations of matrix. Living cells were maintained at 37°C in a 5% CO_2 atmosphere under an inverted microscope (Axiovert 200M; Carl Zeiss, Inc.) equipped with a motorized stage, cooled CCD camera (CoolSNAP HQ2; Roper Scientific), and a live cell imaging plan Apochromat 63× NA 1.2 water immersion objective (Carl Zeiss, Inc.). To minimize the possible photobleaching and light-induced cell damage, the excitation light of a 100-W Hg lamp was reduced to 30% with a FluoArc system (Carl Zeiss, Inc.) and additionally attenuated with a filter (ND75; Carl Zeiss, Inc.). 15 isolated cells were randomly chosen for each experimental condition, and 10–15 control WT cells were recorded simultaneously. Images were acquired, looping all stage positions at 4-min intervals over 6 h. The turnover of FAs located at the cell front was quantified using MetaMorph software. In brief, the adhesion area was outlined on the raw images during steady state, and then adhesion was manually followed from its nucleation. The MFI in the same area was measured, subtracting the background value. Four parameters of adhesion turnover were determined: the total lifetime, the period of steady state, and the rates of assembly and disassembly.

FRAP

MEF cells transiently expressing EGFP-talin or EGFP-vinculin were cultured on LabTekII chambers (Thermo Fisher Scientific) previously coated with either 20 μg/ml FN or 5 μg/ml VN. FRAP experiments were performed with an LSM510 confocal microscope equipped with the on-stage incubator. One individual FA per cell located at the leading edge was processed by FRAP. EGFP fluorescence in the adhesion area was eliminated by 100 bleach cycles at 100% intensity of the 488-nm argon laser. The fluorescence recovery was then sampled with low laser power (2–3%) each minute for 15–20 min. The recovery curves were obtained using MetaMorph software by measuring the MFI in the bleached region and correcting it to the overall image photobleaching. The corrected curve was adjusted with Kaleidagraph software (SynergySoftware) using the mono-exponential fit. The characteristic recovery time, τ, was the mean of at least 20 individual FAs.

Online supplemental material

Fig. S1 shows the distribution of β_3 integrin containing FAs and the expression of adhesion proteins in WT and *Icap-1*–null MEF cells. Fig. S2 shows the spreading and migration on increased FN matrix densities of WT, *Icap-1*–null, and rescued *Icap-1*–null MEF cells. Fig. S3 illustrates the adhesive behavior (cell migration, spreading, and FA dynamics) of WT and *Icap-1*–null MEF cells spread on VN, a β_3 integrin–specific matrix. Fig. S4 shows that β_1-integrin activation in WT MEFs and rescued *Icap-1*–null osteoblasts induces a similar spreading to *Icap-1*–null cells. Online supplemental material is available at http://www.jcb.org/cgi/content/full/jcb.200707142/DC1.

We would like to thank members of the laboratory for all of their input and helpful discussions. We thank E. Planus, J. Torbet, and K. Sadoul for critical reading of the manuscript. We thank G. Chevalier for technical assistance and A. Stuani for imaging assistance.

This work was supported by a grant from the Ligue Nationale Contre le Cancer, the Association de Recherche pour le Cancer, Areca, the Groupement des Entreprises Françaises Monegasques dans la Lutte contre le Cancer, and the Région Rhône-Alpes. A. Millon-Frémillon was supported by a fellowship from the Ministère de l'Education Nationale de la Recherche et de la Technologie.

Submitted: 20 July 2007
Accepted: 26 December 2007

References

Albiges-Rizo, C., P. Frachet, and M.R. Block. 1995. Down regulation of talin alters cell adhesion and the processing of the alpha 5 beta 1 integrin. *J. Cell Sci.* 108:3317–3329.

Bennett, J.S. 2005. Structure and function of the platelet integrin alphaIIbbeta3. *J. Clin. Invest.* 115:3363–3369.

Bershadsky, A.D., N.Q. Balaban, and B. Geiger. 2003. Adhesion-dependent cell mechanosensitivity. *Annu. Rev. Cell Dev. Biol.* 19:677–695.

Bhatt, A., I. Kaverina, C. Otey, and A. Huttenlocher. 2002. Regulation of focal complex composition and disassembly by the calcium-dependent protease calpain. *J. Cell Sci.* 115:3415–3425.

Bouvard, D., and M.R. Block. 1998. Calcium/calmodulin-dependent protein kinase II controls integrin alpha5beta1-mediated cell adhesion through the integrin cytoplasmic domain associated protein-1alpha. *Biochem. Biophys. Res. Commun.* 252:46–50.

Bouvard, D., L. Vignoud, S. Dupe-Manet, N. Abed, H.N. Fournier, C. Vincent-Monegat, S.F. Retta, R. Fassler, and M.R. Block. 2003. Disruption of focal adhesions by integrin cytoplasmic domain-associated protein-1 alpha. *J. Biol. Chem.* 278:6567–6574.

Bouvard, D., A. Aszodi, G. Kostka, M.R. Block, C. Albiges-Rizo, and R. Fassler. 2007. Defective osteoblast function in ICAP-1-deficient mice. *Development.* 134:2615–2625.

Calderwood, D.A. 2004. Integrin activation. *J. Cell Sci.* 117:657–666.

Calderwood, D.A., B. Yan, J.M. de Pereda, B.G. Alvarez, Y. Fujioka, R.C. Liddington, and M.H. Ginsberg. 2002. The phosphotyrosine binding-like domain of talin activates integrins. *J. Biol. Chem.* 277:21749–21758.

Chang, D.D., C. Wong, H. Smith, and J. Liu. 1997. ICAP-1, a novel beta1 integrin cytoplasmic domain-associated protein, binds to a conserved and functionally important NPXY sequence motif of β1 integrin. *J. Cell Biol.* 138:1149–1157.

Chang, D.D., B.Q. Hoang, J. Liu, and T.A. Springer. 2002. Molecular basis for interaction between Icap1 alpha PTB domain and beta 1 integrin. *J. Biol. Chem.* 277:8140–8145.

Chen, C.S., J. Tan, and J. Tien. 2004. Mechanotransduction at cell-matrix and cell-cell contacts. *Annu. Rev. Biomed. Eng.* 6:275–302.

Clark, K., R. Pankov, M.A. Travis, J.A. Askari, A.P. Mould, S.E. Craig, P. Newham, K.M. Yamada, and M.J. Humphries. 2005. A specific alpha-5beta1-integrin conformation promotes directional integrin translocation and fibronectin matrix formation. *J. Cell Sci.* 118:291–300.

Cluzel, C., F. Saltel, J. Lussi, F. Paulhe, B.A. Imhof, and B. Wehrle-Haller. 2005. The mechanisms and dynamics of αvβ3 integrin clustering in living cells. *J. Cell Biol.* 171:383–392.

Czuchra, A., H. Meyer, K.R. Legate, C. Brakebusch, and R. Fassler. 2006. Genetic analysis of β1 integrin "activation motifs" in mice. *J. Cell Biol.* 174:889–899.

Discher, D.E., P. Janmey, and Y.L. Wang. 2005. Tissue cells feel and respond to the stiffness of their substrate. *Science.* 310:1139–1143.

Engler, A.J., S. Sen, H.L. Sweeney, and D.E. Discher. 2006. Matrix elasticity directs stem cell lineage specification. *Cell.* 126:677–689.

Ezratty, E.J., M.A. Partridge, and G.G. Gundersen. 2005. Microtubule-induced focal adhesion disassembly is mediated by dynamin and focal adhesion kinase. *Nat. Cell Biol.* 7:581–590.

Fournier, H.N., S. Dupe-Manet, D. Bouvard, M.L. Lacombe, C. Marie, M.R. Block, and C. Albiges-Rizo. 2002. Integrin cytoplasmic domain-associated protein 1alpha (ICAP-1alpha) interacts directly with the metastasis suppressor nm23-H2, and both proteins are targeted to newly formed cell adhesion sites upon integrin engagement. *J. Biol. Chem.* 277:20895–20902.

Franco, S.J., M.A. Rodgers, B.J. Perrin, J. Han, D.A. Bennin, D.R. Critchley, and A. Huttenlocher. 2004. Calpain-mediated proteolysis of talin regulates adhesion dynamics. *Nat. Cell Biol.* 6:977–983.

Giannone, G., G. Jiang, D.H. Sutton, D.R. Critchley, and M.P. Sheetz. 2003. Talin1 is critical for force-dependent reinforcement of initial integrin-cytoskeleton bonds but not tyrosine kinase activation. *J. Cell Biol.* 163:409–419.

Ginsberg, M.H., A. Partridge, and S.J. Shattil. 2005. Integrin regulation. *Curr. Opin. Cell Biol.* 17:509–516.

Gupton, S.L., and C.M. Waterman-Storer. 2006. Spatiotemporal feedback between actomyosin and focal-adhesion systems optimizes rapid cell migration. *Cell.* 125:1361–1374.

Han, J., C.J. Lim, N. Watanabe, A. Soriani, B. Ratnikov, D.A. Calderwood, W. Puzon-McLaughlin, E.M. Lafuente, V.A. Boussiotis, S.J. Shattil, and M.H. Ginsberg. 2006. Reconstructing and deconstructing agonist-induced activation of integrin alphaIIbbeta3. *Curr. Biol.* 16:1796–1806.

Hughes, P.E., F. Diaz-Gonzalez, L. Leong, C. Wu, J.A. McDonald, S.J. Shattil, and M.H. Ginsberg. 1996. Breaking the integrin hinge. A defined structural constraint regulates integrin signaling. *J. Biol. Chem.* 271:6571–6574.

Hynes, R.O. 2002. Integrins: bidirectional, allosteric signaling machines. *Cell.* 110:673–687.

Ingber, D.E. 2003. Mechanosensation through integrins: cells act locally but think globally. *Proc. Natl. Acad. Sci. USA.* 100:1472–1474.

Jiang, G., G. Giannone, D.R. Critchley, E. Fukumoto, and M.P. Sheetz. 2003. Two-piconewton slip bond between fibronectin and the cytoskeleton depends on talin. *Nature.* 424:334–337.

Kaverina, I., O. Krylyshkina, and J.V. Small. 1999. Microtubule targeting of substrate contacts promotes their relaxation and dissociation. *J. Cell Biol.* 146:1033–1044.

Leucht, P., J.B. Kim, J.A. Currey, J. Brunski, and J.A. Helms. 2007. FAK-mediated mechanotransduction in skeletal regeneration. *PLoS ONE.* 2:e390.

Liddington, R.C., and M.H. Ginsberg. 2002. Integrin activation takes shape. *J. Cell Biol.* 158:833–839.

Luo, B.H., T.A. Springer, and J. Takagi. 2004. A specific interface between integrin transmembrane helices and affinity for ligand. *PLoS Biol.* 2:e153.

Martel, V., C. Racaud-Sultan, S. Dupe, C. Marie, F. Paulhe, A. Galmiche, M.R. Block, and C. Albiges-Rizo. 2001. Conformation, localization, and integrin binding of talin depend on its interaction with phosphoinositides. *J. Biol. Chem.* 276:21217–21227.

Partridge, A.W., S. Liu, S. Kim, J.U. Bowie, and M.H. Ginsberg. 2005. Transmembrane domain helix packing stabilizes integrin alphaIIbbeta3 in the low affinity state. *J. Biol. Chem.* 280:7294–7300.

Paszek, M.J., N. Zahir, K.R. Johnson, J.N. Lakins, G.I. Rozenberg, A. Gefen, C.A. Reinhart-King, S.S. Margulies, M. Dembo, D. Boettiger, et al. 2005. Tensional homeostasis and the malignant phenotype. *Cancer Cell.* 8:241–254.

Priddle, H., L. Hemmings, S. Monkley, A. Woods, B. Patel, D. Sutton, G.A. Dunn, D. Zicha, and D.R. Critchley. 1998. Disruption of the talin gene compromises focal adhesion assembly in undifferentiated but not differentiated embryonic stem cells. *J. Cell Biol.* 142:1121–1133.

Raftopoulou, M., and A. Hall. 2004. Cell migration: Rho GTPases lead the way. *Dev. Biol.* 265:23–32.

Sakai, T., Q. Zhang, R. Fassler, and D.F. Mosher. 1998. Modulation of β1A integrin functions by tyrosine residues in the β1 cytoplasmic domain. *J. Cell Biol.* 141:527–538.

Schober, M., S. Raghavan, M. Nikolova, L. Polak, H.A. Pasolli, H.E. Beggs, L.F. Reichardt, and E. Fuchs. 2007. Focal adhesion kinase modulates tension signaling to control actin and focal adhesion dynamics. *J. Cell Biol.* 176:667–680.

Tadokoro, S., S.J. Shattil, K. Eto, V. Tai, R.C. Liddington, J.M. de Pereda, M.H. Ginsberg, and D.A. Calderwood. 2003. Talin binding to integrin beta tails: a final common step in integrin activation. *Science.* 302:103–106.

Takagi, J., and T.A. Springer. 2002. Integrin activation and structural rearrangement. *Immunol. Rev.* 186:141–163.

Vinogradova, O., J. Vaynberg, X. Kong, T.A. Haas, E.F. Plow, and J. Qin. 2004. Membrane-mediated structural transitions at the cytoplasmic face during integrin activation. *Proc. Natl. Acad. Sci. USA.* 101:4094–4099.

Webb, D.J., K. Donais, L.A. Whitmore, S.M. Thomas, C.E. Turner, J.T. Parsons, and A.F. Horwitz. 2004. FAK-Src signalling through paxillin, ERK and MLCK regulates adhesion disassembly. *Nat. Cell Biol.* 6:154–161.

Zaidel-Bar, R., R. Milo, Z. Kam, and B. Geiger. 2007. A paxillin tyrosine phosphorylation switch regulates the assembly and form of cell-matrix adhesions. *J. Cell Sci.* 120:137–148.

Zhang, X.A., and M.E. Hemler. 1999. Interaction of the integrin beta1 cytoplasmic domain with ICAP-1 protein. *J. Biol. Chem.* 274:11–19.